Oscillatory solutothermal convection-driven evaporation kinetics in colloidal nanoparticle-surfactant complex fluid pendant droplets

A. R. Harikrishnan,[1,*] Purbarun Dhar,[2,†] Sateesh Gedupudi,[1] and Sarit K. Das[2,‡]
[1]*Department of Mechanical Engineering, Indian Institute of Technology Madras, Chennai, 600036, India*
[2]*Department of Mechanical Engineering, Indian Institute of Technology Ropar, Rupnagar, Punjab, 140001, India*

(Received 21 October 2017; published 25 July 2018)

To elucidate the pure physics of evaporation which is free from surface effects, the pendant mode of evaporation is employed in the present study. The present study brings out the evaporation kinetics of a combined surfactant and nanoparticle colloidal system. We also segregate the contributing effects of surfactants alone, particle alone, and the combined effect of surfactant and particles in modulating the evaporation kinetics. It is observed that the rate of evaporation is a strong function of the particle concentration for nanocolloidal suspensions of particle alone and concentration of surfactant molecules up to the micellar concentration and thereafter insensitive to concentration for an aqueous surfactant solution. The combined colloidal system of nanoparticles and surfactant exhibited the maximum evaporation rate, and the rate is a strong function of the concentration of both the particle and surfactant. The theoretical classical diffusion-driven evaporation falls short of the experimentally observed evaporation rate in aqueous surfactant and colloidal solutions. Evidence of convective currents was observed in flow visualization studies in aqueous surfactant solutions, nanocolloidal solution of particle alone, and an oscillatory convective circulation in a combined surfactant-impregnated nanocolloidal solution. Thermal Marangoni and Rayleigh numbers are calculated from the theoretical examination and are found not potent enough to induce strong circulation currents in such systems from a stability map. Scaling analysis of solutal Marangoni is observed to be capable of inducing circulation from a stability map in all the systems and the enhanced thermophoretic drift and Brownian dynamics, and enhancement in the diffusion coefficient of the nanoparticles is also contributing to the enhanced evaporation rate for only nanocolloidal solutions. The oscillatory convective current arising out of two opposing driving potential enhances the evaporation rate of surfactant-impregnated nanocolloids. The present findings could reveal the effect of surfactants in tuning the evaporation rate of colloidal solutions.

DOI: 10.1103/PhysRevFluids.3.073604

I. INTRODUCTION

The fundamental physics behind the phenomenon of evaporation kinetics finds application in various domains, for instance, in furnace and internal combustion engines and in heat transfer equipment involving phase change [1,2]. According to Maxwell's definition, the evaporation is a pure diffusion-driven mechanism [3]. Recent developments in desalination, painting, cooling technologies, and even biological domains such as DNA synthesis and patterning technologies have ignited a renewed interest in the field of evaporation [4–6]. Driven by the unique thermophysical

*Corresponding author: harianilakkad@gmail.com
†purbarun@iitrpr.ac.in
‡skdas@iitrpr.ac.in

properties, intensive research has been undertaken to study the fundamentals behind the suspensions of nanosized colloidal dispersions in various fields for the past two decades [7–10]. A thorough understanding of the evaporation dynamics and the physics behind the process is essential to extend the process to such applications so as to effectively utilize the properties of these *smart fluids*.

In general most of the studies on evaporation are limited to sessile droplet evaporation characteristics, and extensive study has been conducted on sessile water droplet evaporation, notably by Picknett and Bexon, Deegan, Popov, *et al.* [11–13] in order to understand the physics of heat and mass transfer across the interface. There are few studies on the evaporation characteristics of complex nanofluids to trace the phenomenon in the case of such multicomponent fluids [14–16]. When it comes to the case of such complex multicomponent fluids, the real physics of the evaporation mechanism can be elucidated only with the pendant mode of evaporation where the surface effects do not come into picture. Especially in a complex colloidal system consisting of suspended nanoparticles and the stabilizing agents such as surfactants, the surfaces play a predominant role [7]. There can be adsorption and other interactions which can drastically alter the evaporation physiognomies and result in a paradigm shift in the modes of interfacial transfer process [7,17]. The presence of foreign surfactant molecules in colloidal systems drastically alters the interfacial properties [7,8,18], which can cause serious implications for the evaporation rate.

Even though there are a few studies [15,19] on the evaporation mechanism in such complex colloidal systems and very few attempts to understand the physics of evaporation in surfactant solutions, the combined effect of surfactants and particles in altering the rate of interfacial mass transport has not been reported yet to the best of the authors' knowledge. A suspended droplet method to characterize the droplet evaporation characteristics has been in practice among researchers for a long time [20]. There are few studies which probe the evaporation mechanism in aqueous surfactant solutions [21,22]. All the studies on aqueous surfactant solutions are limited to the sessile mode of evaporation and are prone to surface effects especially for the interface active agents like surfactants. The studies reported an enhancement in evaporation rate with respect to the concentration of the surfactants. Gerken *et al.* [19] observed that the presence of aluminum nanoparticles in ethanol droplets reduce the evaporation rate with particle concentration and reported that the nanoparticle agglomerate packing near the evaporating droplet surface resulted in the reduction of the liquid fraction available for evaporation. The effects of dynamic concentration of the nanocolloids have been observed by Chen *et al.* [15] who noticed a transition in the evaporation rate constant from one value to another. They attributed the change in evaporation rate constant of different fluids to the change in latent heat of vaporization.

The present study experimentally evaluates the effect of surfactant molecules, nanoparticles, and the combined effect of surfactants and nanoparticles in modulating the evaporation kinetics of pendent droplets in quiescent ambience. The present study attempts to gain insight into the physics of the interplay of surfactants and particles in altering the evaporation characteristics as the present study is free from any surface effects. Particle image velocimetry (PIV) studies are performed to understand exactly how the presence of foreign surfactant and nanoparticles modulates internal circulation within the droplets and how it directly correlates to the evaporation rate. Thermal Marangoni and Rayleigh numbers are calculated from the theoretical scaling examination. The present findings are useful for tuning the performance of many engineering devices at the macro- and microlevel where phase change heat transfer is of prime importance.

II. EXPERIMENTS

A. Materials

The experiments in the present work are envisaged in such a way as to demarcate and segregate the contribution of each parameter influencing the evaporation kinetics of nanosuspensions, *viz.* nanoparticle concentration, surfactant nature and concentration, and nanoparticle-surfactant interactions. Deionized (DI) water (polar, Millipore, 1–3 μS/cm) and three types of metal oxide nanoparticles—CuO (30 nm, NanoArc), Al_2O_3 (20 nm, Nanoshel Inc. USA), and SiO_2 ($\sim$10 nm,

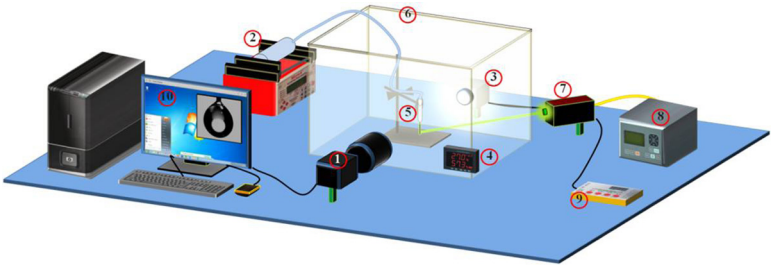

FIG. 1. Illustration of the experimental setup: (1) camera with a lens system, (2) syringe pump, (3) backlight with a diffuser, (4) temperature and humidity sensor, (5) syringe and needle system to generate pendant drop, (6) controlled enclosure chamber, (7) laser with a plano-convex lens, (8) laser power control unit, (9) backlight control unit, and (10) computer system.

Alfa Aeser, India)—have been considered in the present investigation. Carbon-based nanocolloidal systems, *viz.* multiwalled carbon nanotubes (MWCNT) (60-80 nm external diameter and aspect ratio ∼100, Sisco Research Lab, India) and *in situ* prepared graphene are also considered in the present investigation.

Figure S1 in the Supplemental Material illustrates the High-Resolution Scanning Electron Microscopy image of different particles [23]. In the present study, sodium dodecyl sulphate (SDS, 99% pure, Sisco Research Labs, India) has been chosen as the anionic surfactant, whereas cetyltrimethylammonium bromide (CTAB) (99% pure, Sisco Research Labs, India) has been chosen as the cationic counterpart. Graphene is prepared *in situ* using the two-step process invoking the modified Hummer's method. The detailed procedure is described in the reported literature [24]. The confirmation of the presence of graphene is evident from the presence of a 2D band at $\sim 2800\,\mathrm{cm}^{-1}$ and the ratio of intensity of the 2D to G band is around 0.35 to 4.5, indicating three or four layers of graphene [25]. See the Supplemental Material for details of dynamic light scattering (DLS) and zeta potential characterization of nanoparticles [23].

B. Experimental methodology

The first run of experiments has been conducted with only the base fluid, DI water, so that the reference datum for comparison is obtained. Second, the effect of dispersing the so-called surface active agents due to its strong interfacial effects are investigated by studying the evaporation kinetics of the aqueous surfactant pendant droplet alone. The Critical Micelle Concentration (CMC) values are fixed from our previous reported literature [7], and the surfactant concentration is expressed in a nondimentionalized normalized form throughout this paper in the form as $C_s = C/C_{\mathrm{CMC}}$ for each of the surfactants considered. Aqueous solutions of SDS and CTAB are prepared at different concentration levels ranging from $C_s = 0.25$ to $C_s = 5$ so that the transfer characteristics of premicellar, micellar, and postmicellar solutions can be captured. In order to obtain the contribution induced by particles, experiments have been conducted by preparing the nanofluids without using surfactants. CuO-, Al_2O_3-, and SiO_2-based dispersions have been considered for the present study. A detailed procedure for preparation of nanoparticles is described in detailed in the previous literature [7]. The fourth set of experimental runs is conducted on nanofluids prepared with surfactants which act as stabilizing agents in which the influence of base fluid, surfactants, and nanoparticles are present simultaneously. The experiments are conducted at different particle concentrations, and each of the samples has been prepared at three surfactant concentrations of $C_s = 0.25$, 0.5, and 1 for each surfactant.

Figure 1 illustrates the experimental setup developed for the present study to understand the evaporation rate and flow kinetics in an evaporating pendant drop. The droplets are suspended with a syringe pump (New Era Pump Systems Inc., USA) connected to a 27 gauge needle at the other end so as to dispense accurate volume of pendant droplet. The droplet is generated in a closed

acrylic chamber so that the stray convection effect will not perturb the evaporation. Provision has been made to measure the humidity and the temperature of the test cell enclosure chamber. A CCD camera (Holmarc Optomechatronics, India) coupled with a zoom lens and backlight arrangement is used for capturing the video frames. Diffuser arrangement has been provided to reduce the effect of backlight on the evaporation rate. As all droplets are subjected to same source intensity of light, it will not affect comparison of the evaporation rate. In order to qualitatively track the internal circulation if any and to get a quantitative picture of the internal circulation mechanism, flow visualization is employed using a two-frame cross correlation PIV. A diode laser (Holmark Optomechatronics, India) is used to illuminate the target area employing a plano-convex lens for generating a light sheet across the droplet. The 532 nm laser has a maximum power rating of 10 mW. The influence of the laser illumination on the evaporation rate is also tested as a control experiment. It is observed that laser illumination for 20 sec (time period for which PIV studies are performed) has a negligible influence on evaporation kinetics (maximum increment in evaporation rate of 2%–3%). Neutrally buoyant fluorescent particles with an average diameter of 25 μm are used as seed particles, and throughout the experiment the concentration of the seed particles is kept at about 0.05 vol%. The temperature and relative humidity in the test cell chamber are maintained at 27 ± 1 °C and 55% ±5%, respectively. For the visualization experiments, the frame rate is kept at 10 per second. The images were processed with the open-source "PIV-LAB" software [26,27] to obtain the velocities. The images were well correlated, with a correlation coefficient greater than 0.75.

III. RESULTS AND DISCUSSION

A. Evaporation characteristics of aqueous surfactant solutions and nanocolloids

Figure 2(a) illustrates the normalised square of diameter $\Psi = \frac{D^2}{D_o^2}$ of the aqueous surfactant pendant drop variation with the time factor $\tau = \frac{t}{D_0^2}$. D_o represents the spherical equivalent diameter (mm) of the pendant droplet at the beginning of evaporation, and D represents the spherical equivalent diameter (mm) at any time t (sec). The diameter of a spherical drop with same volume as the pendant drop is the equivalent diameter. It can be observed that Ψ decreases linearly with the τ at all normalized surfactant concentrations for an aqueous CTAB solution (similar behavior observed in the case of SDS also). It can be elucidated that the D^2 law (see Supplemental Material for details [23,28]) is valid in the case of aqueous surfactant solutions as

$$\Psi = 1 - k\tau, \tag{1}$$

where k is the evaporation rate constant. The rate of evaporation increases up to the micellar concentration, and after the micellar concentration the rate remains almost constant as illustrated in Fig. 2(b). The addition of extra surfactant even up to five times the micellar concentration after micellar concentration could not bring any appreciable change in evaporation characteristics. The interesting part of the problem is that the evaporation rate is dependent on the concentration of the surfactant as we can observe in Fig. 2.

As the evaporation proceeds, only the aqueous solution gets evaporated and the surfactant molecules remain in the solution. Since the D^2 law evaluation is based on the vapor side analysis as outlined by Abramzon and Sirignano [29], the D^2 law is valid in the aqueous surfactant solution cases also as illustrated in Fig. 2 at all concentrations of surfactants. The inset in Fig. 2(b) illustrates the snapshots of the pendant drops at various instants of time factor τ for water and aqueous SDS surfactant solutions of concentrations $C_s = 0.25$ and $C_s = 1.0$. It can be clearly observed that the evaporation proceeds much faster in the case of surfactant solutions and the rate increases with the increase in surfactant concentration.

To understand the effect of suspended nanocolloidal particles on the evaporation kinetics of nanocolloidal suspensions, experiments are conducted with colloidal solutions with only particles without the aid of any surfactants. Figure 3 illustrates the nature of variation of ψ with τ for different nanocolloidal solutions. It can be observed that the complex nanocolloidal solutions follow the D^2 law as ψ varies linearly with τ. As the analysis of the gas phase of the evaporating droplet is

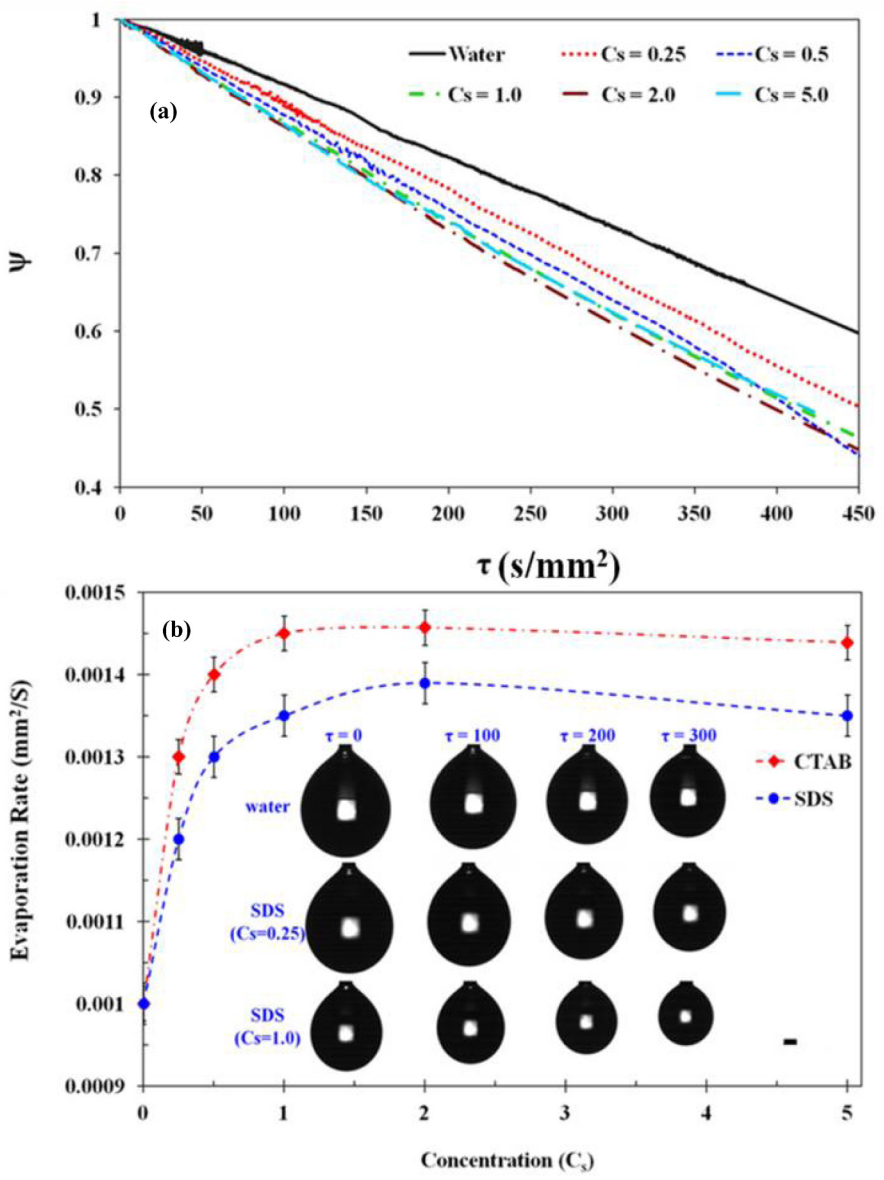

FIG. 2. (a) Plot of nondimensional square of diameter with the time factor τ for CTAB; (b) variation of the experimental evaporation rate constant with SDS and CTAB concentration. The scale bar represents 0.406 mm.

considered in arriving at the D^2 law, the validity of D^2 law for the complex colloidal solutions can be justified. The nature of evaporation kinetics exhibited by different nanocolloidal solutions is similar. The nanocolloids are found to exhibit a higher evaporation rate compared to that of the base fluid, and the rate of evaporation is a strong function of the concentration, nature, and characteristics of the suspended phase.

The nature of variation of the instantaneous rate constant of evaporation k with τ is illustrated in Fig. 3(b) for CuO nanocolloidal suspensions at a concentration of 0.08 vol%. The average value of the rate constant can be considered to be constant with time. The evaporation rate monotonously increases with the particle concentration for all the particles, and the rate of increase is high

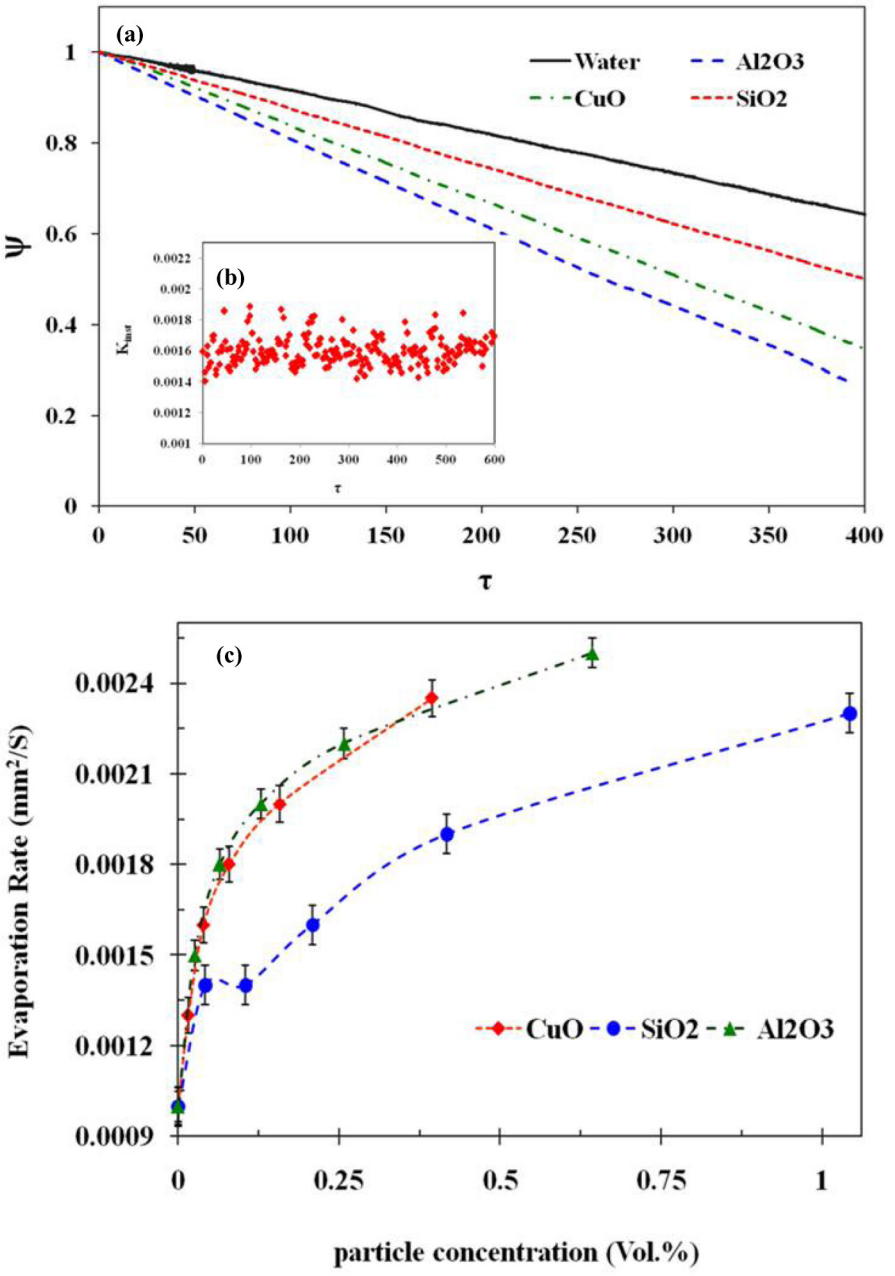

FIG. 3. (a) Evaporation characteristics of only nanocolloidal solutions of CuO, Al_2O_3, and SiO_2 at concentrations of 0.04, 0.065, and 0.11 vol%, respectively. (b) The instantaneous variation of the evaporation rate constant (K_{inst}) with the time factor τ for CuO nanocolloidal solutions at a concentration of 0.04 vol%. (c) Variation of the evaporation rate constant with the particle concentration for various nanocolloidal solutions.

at lower concentration of the particle. As the concentration of the particle increases towards higher concentration, the change in evaporation rate with particle concentration decreases. Al_2O_3 nanocolloids showed the maximum enhancement in evaporation rate compared to other particles, at all concentrations of particles considered. SiO_2 nanocolloids showed the minimum increment in

evaporation rate from the base fluid. It can be elucidated that the rate of evaporation is a strong function of the nature, and the characteristics of the suspended phase as the evaporation rate varies for different nanocolloidal systems.

B. Evaporation kinetics of combined particle and surfactant colloidal systems

In order to probe the physics of evaporation kinetics of combined nanocolloidal systems in the presence of surfactants, experiments were conducted with colloidal solutions impregnated with surfactant molecules at different particle and surfactant concentrations of nanocolloidal suspensions keeping one of the concentrations constant. The study conducted at different concentrations of surfactants and particles will help to elucidate the influence and contributions of individual components and the net total effect in amending the nature of evaporation kinetics. As the evaporation is a surface phenomenon, the interface plays an important role, and the presence of strong surface active agents bonded to the nanoparticles can drastically alter the interfacial energetics. It is a well-established fact that the surfactants are capable of altering the interfacial energies due to the adsorption to the interfaces [7]. Due to the interfacial adsorption, the surfactants lower the interface energies of the aqueous solution and decreases with the concentration of surfactant molecules up to the micellar concentration [7]. Nanocolloidal solutions of only particles showed an increment in surface tension with the particle concentration [7]. The rate of increment is higher at the lower concentration of the particle, whereas it decreases towards higher particle concentration. The physics of interaction of the combined particle and surfactant is a very complex phenomenon and can drastically alter the interfacial phenomenon. Recently there are few studies probing the physics of the effect of nanodispersions on the interfacial tension [7,30] and the fate of the nanodispersed phase at the liquid-air interface [29,31]. A recent research work carried out by the present authors [7] concluded that the combined particle and surfactant system exhibited a surface tension different from that of the only particle case and only aqueous surfactant case. It was observed that the combined effect is not additive of individual effects on interfacial phenomenon. The combined system displayed an interfacial tension lower than that exhibited by aqueous surfactant solution. An enhanced population of surfactant molecules at the interface due to nanoparticle-driven enhanced transport to interface [7] was outlined to be the main mechanism responsible for such an anomalous behavior. Because of the inherent affinity of the surfactant molecules to the interface and the combined surfactant-capped particle being in dynamic equilibrium due to thermal fluctuations the combined colloidal system will facilitate in populating the interface with more surfactant molecules and hence result in further reduction of the interfacial tension. The surface tension decreases initially with particle concentration and then almost negligible change with respect to particle concentration at a given surfactant concentration due to the steric hindrance preventing the further adsorption to the interface.

Figure 4(a) illustrates the nature of variation of the square of the normalized diameter with the time factor τ for the base case of water, aqueous surfactant solutions, nanocolloidal solutions, and surfactant-infused nanocolloidal solutions at various concentrations of surfactant and particle as indicated. The CTAB at a concentration of $C_s = 0.25$ exhibits a higher evaporation rate than that compared to the aqueous SDS solution at the same concentration. The 0.25 vol% nanocolloidal solution of Al_2O_3 solution exhibits a higher evaporation rate compared to the aqueous surfactant solutions as illustrated in Fig. 4(a).

However, it is interesting to note that the surfactant-infused nanocolloids recorded an evaporation rate much higher than the only aqueous surfactant solution and only nanocolloidal solution. The combined nanocolloidal solution of Al_2O_3 and CTAB exhibited an evaporation rate much higher than only Al_2O_3 nanocolloidal solution and aqueous CTAB solution. Among the three combined nanocolloidal solutions considered in the present study, the graphene and SDS-based nanocolloidal solution indicated the maximum evaporation. Even though the surface tension is not additive in the case of combined colloidal systems, the evaporation rate is found to be additive in the case of a combined colloidal solution as both the aqueous surfactant solution and the nanocolloidal solution of only particles are aiding in enhancing the evaporation rate independently. It is interesting to note

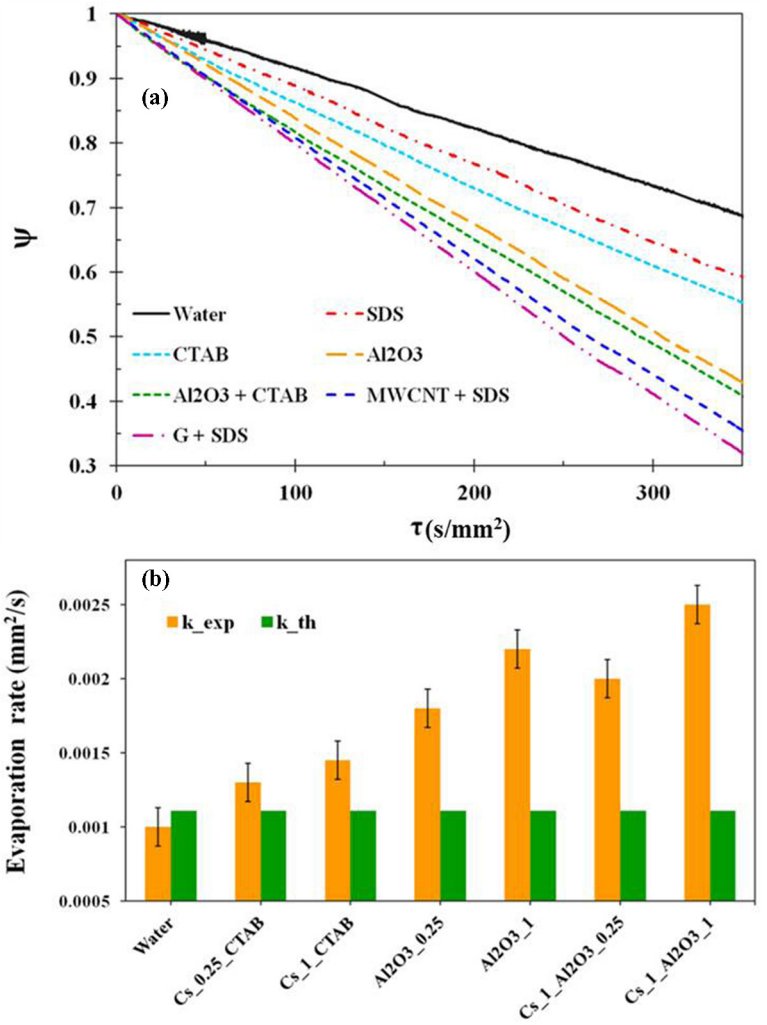

FIG. 4. (a) Nature of variation of the square of the normalized diameter of the droplet with the time factor τ for surfactant solutions at a concentration of $C_s = 0.25$ and the Al_2O_3 nanocolloid at a particle concentration of 0.25 vol% and for surfactant-infused nanocolloids. (b) Experimentally observed (K_{exp}) and calculated diffusion-driven evaporation rate (K_{th}) for different complex fluids.

that the nature and the characteristics of the nanosuspension affect the evaporation kinetics as the rate of evaporation is different for the graphene and SDS-based nanosuspension and MWCNT and SDS-based nanosuspension both being at the same concentration of particle and surfactant. The D^2 law is obeyed by the combined nanocolloidal suspensions as illustrated in Fig. 4(a) as the ψ is varying linearly with the time factor τ. Figure 5 illustrates the surface plot demonstrating the nature of variation of the experimentally observed evaporation rate constant with the particle and surfactant concentration for the Al_2O_3 and CTAB-based nanocolloids, MWCNT and SDS-based nanocolloids, and graphene and SDS-based nanocolloids. For a given particle concentration, with the increase in surfactant concentration, the evaporation rate constant increases. The rate of increase is more pronounced at the lower surfactant concentrations, and towards higher surfactant concentration, the rate of increment is lower. This trend is similar for all particle concentrations. For a given surfactant concentration, the evaporation rate constant increases with the increase in particle concentration.

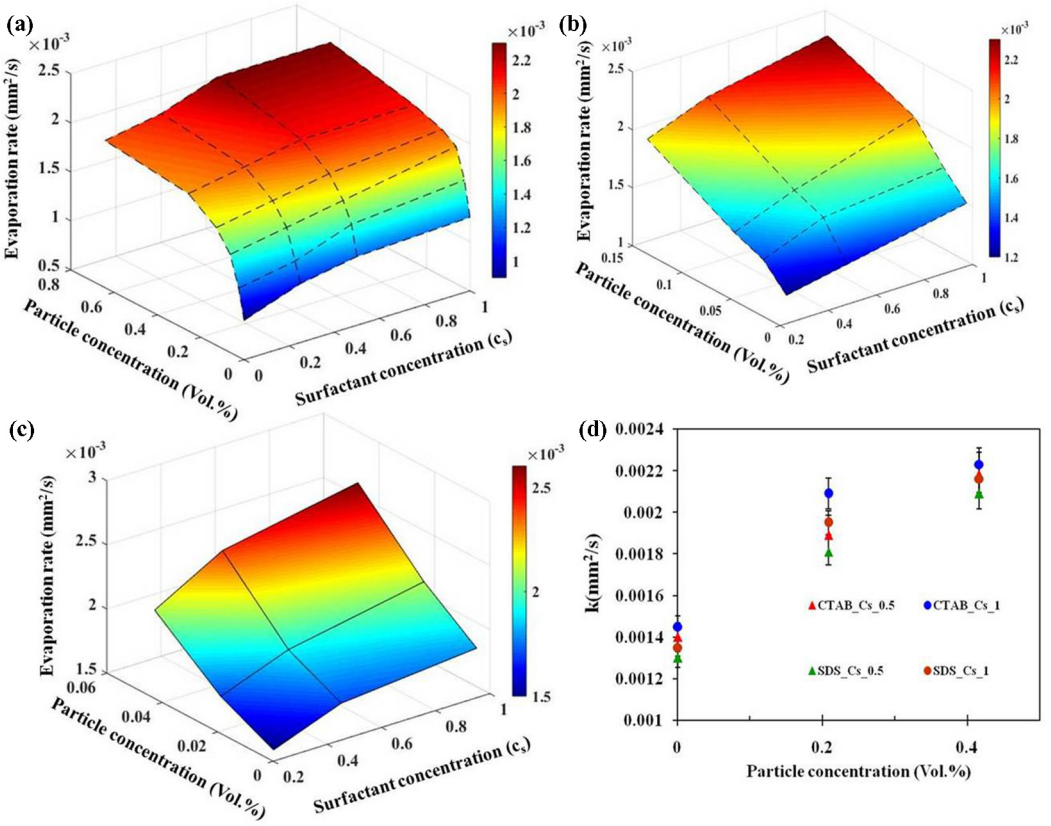

FIG. 5. Surface plot illustrating the variation of the experimentally observed evaporation rate constant with the particle and surfactant concentration for (a) CTAB-infused Al_2O_3, (b) SDS-infused MWCNT, and (c) SDS-infused graphene nanocolloids. (d) Evaporation rate of SiO_2 nanocolloid infused with SDS and CTAB surfactant.

Similar to the behavior with respect to the surfactant concentration, at a given surfactant concentration the rate of increment in the evaporation rate constant is high at lower particle concentration and the rate of increment decreases towards higher particle concentration. This trend is the same at all levels of surfactant concentration. This nature of variation of the evaporation rate is common to all the combined particle and surfactant colloidal systems considered in the present study.

The theoretical diffusion-driven evaporation rate according to Abramzon and Sirignano [29] (see the Supplemental Material for details [23]) and the experimentally observed evaporation rate is represented in Fig. 4(b). The theoretical model fairly matches with the water case, whereas it does not match for aqueous surfactant solutions, nanocolloids of particle alone, and combined surfactant and particle-impregnated nanocolloidal solutions as illustrated in Fig. 4(b). The theoretical diffusion-driven evaporation rate under predicting the experimentally observed evaporation rate implies that there are other mechanisms influencing the evaporation of these complex fluids in addition to the diffusion mechanism.

Evaporation studies have been performed with SiO_2-based nanocolloids with both CTAB and SDS surfactants as it is stable with both the surfactants so that the effect of electrostatic complexing can be explored. SiO_2 with CTAB forms a complexing system of nanocolloidal dispersions, and SiO_2 with SDS forms a noncomplexing system of nanocolloidal system. The complexing system is found to exhibit a higher evaporation rate compared to the noncomplexing system. However, the

differences between both the systems are found to be small. The rate is found to increase with the surfactant and particle concentration. This clearly indicates the pronounced effect of surfactants in the case of surfactant-infused nanocolloids as also observed in previous studies on interfacial characteristics. The complexing system mechanism is described in detail in the later part of the discussion. The noncomplexing system behaves similarly to a surfactant system but with a slightly higher evaporation rate because of the presence of particle which can induce other mechanisms along with that present in the only surfactant case as described in a later section.

C. Exploring physics of enhanced evaporation: Internal circulation from flow visualization studies

For better understanding of the physics of enhanced evaporation characteristics and to figure out the mechanisms behind this, flow visualization experiments have been carried out in different complex fluids. As a base case, experiments on a water droplet revealed that there is no observable circulation. The maximum magnitude of the circulation velocity vector is found to be 0.018 cm/sec. The observations are in line with that of the earlier reported literature on evaporation characteristics of water and multicomponent fluids by Mandal *et al.* [20]. Hence it can be concluded that there is no circulation in the case of water, and the evaporation mechanism is purely diffusion-driven. The study extended to the surfactant solutions showed internal circulation within the fluid droplet. It can be observed from Fig. 6(a) that the circulation cell of a definite pattern is formed at a surfactant concentration of $C_s = 0.25$. The maximum magnitude of the velocity vector obtained by the postprocessing is 0.2 cm/sec. However, moving on to a higher surfactant concentration of $C_s = 0.5$, two cells of internal circulation are observed as illustrated in Fig. 6(c). Also the cells change the direction of rotation periodically. The flow visualization analysis performed and illustrated in Fig. 7 is taken after 30 sec from the start of experiment. These two definite cells are circulating in opposite directions at a given point of time. On further increase of surfactant towards the micellar concentration, a larger circulation cell with an enhanced circulation is observed. The convection current observed is so strong in this case as the maximum velocity vector magnitude is about three times as observed in the case of the one-fourth micellar concentration droplet. The flow visualization experiments are not carried out to higher concentration of the surfactant concentration thereafter as the post micellar region is of not much interest to the present study. Hence the enhanced evaporation characteristics of the aqueous surfactant solutions can be attributed to the presence of internal circulation. Figure 6(d) illustrates the nature of variation of the circulation velocity with time for the surfactant solution. It can be observed that the mean magnitude of the velocity remains constant with time. The fluctuations correspond to the noise levels in the measurement of velocity.

The flow visualization in nanocolloidal solutions is very difficult to realize due to the complexity and the presence of dispersed particles in the suspension. In the present study the flow visualization is carried out for the Al_2O_3 nanocolloids at a particle concentration of 0.0125 vol%. This was the maximum particle concentration with which the flow was observable, and hence the study was limited to only one particle concentration. Higher concentration makes the fluid opaque to the presence of particles. The method of flow visualization gives a general picture of the flow pattern even though the dispersed phase particle and flow visualization particle interactions may be there. The visualization study revealed a slight circulation current present in the droplet and the velocity of the circulation current is weak as illustrated in Fig. 7(a). Figure 6(d) illustrates the nature of variation of the circulation velocity with time for nanocolloidal suspensions. It can be observed that the velocity remains almost steady with respect to time. The flow visualization in the combined surfactant and particle case yielded interesting results as illustrated in Figs. 7(b) and 7(c). An oscillatory convection pattern is exhibited by the droplet in the case of surfactant-infused nanocolloids. The system is subjected to driving forces of opposite motive. One force tries to drive the convection in one direction, whereas another force tries to retard it and the convection starts in another direction. The phenomenon is discussed later in detail.

Figure 7(c) illustrates the nature of variation of the circulation velocity with time for a few seconds. The velocity variations showed some random fluctuations, and the magnitude of fluctuations is

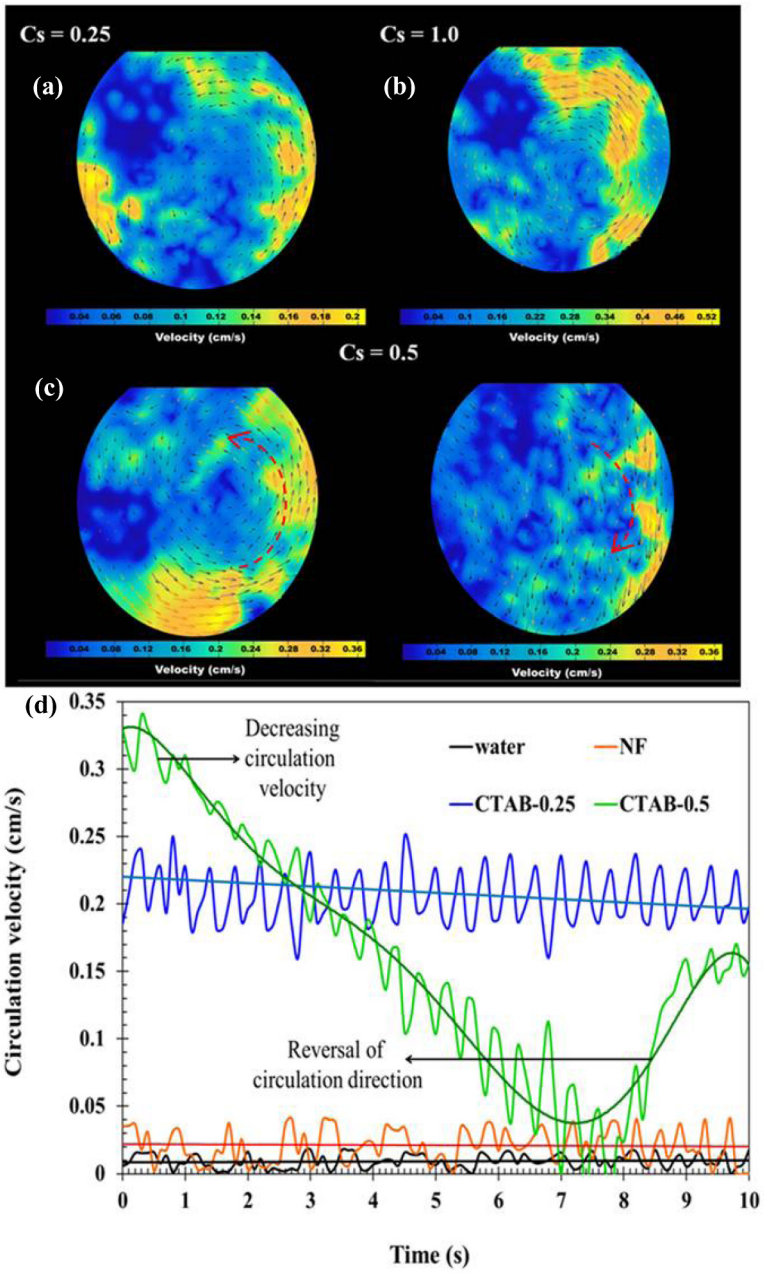

FIG. 6. Postprocess PIV analysis of internal circulation velocity vector plot for aqueous CTAB solution at normalized concentrations of (a) $C_s = 0.25$, (b) $C_s = 1.0$, and (c) $C_s = 0.5$ with reversal dynamics of internal circulation pattern. (d) Variation of the measured circulation velocity with time in the case of water and aqueous CTAB solution at concentrations of $C_s = 0.25$ and $C_s = 0.5$ and for the Al_2O_3 nanocolloidal solution at a particle concentration of 0.0125 vol%.

comparable to that observed in the case of surfactants. The enhanced evaporation kinetics of the surfactant-impregnated nanocolloids can be attributed to the oscillatory convection developed in the droplets. The observed enhanced evaporation rate in droplets can be explained based on the formation

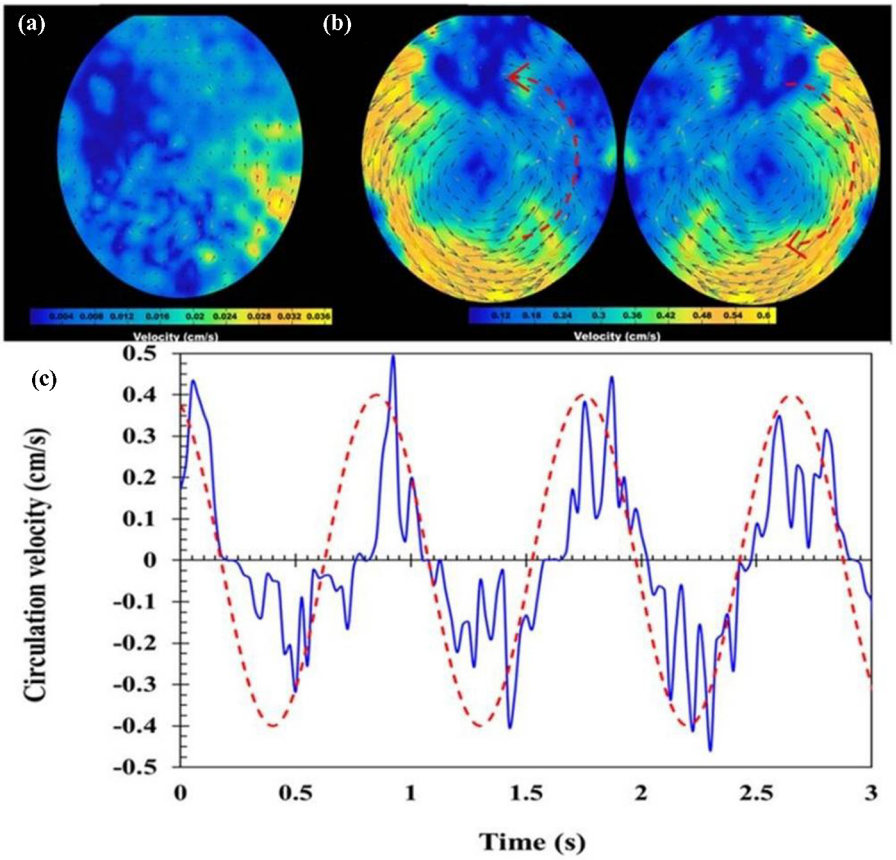

FIG. 7. Velocity contours showing the velocity vectors for (a) nanocolloids without surfactants, (b) surfactant-infused nanocolloids exhibiting an oscillatory convection current, and (c) variation of the circulation velocity with time for CTAB-infused Al_2O_3 nanocolloid at a particle concentration of 0.0125 vol% and surfactant concentration of $C_s = 1.0$.

of the boundary layer on the surface of the droplet [20]. The shear stress developed on the droplet surface due to the internal circulation constantly entrains the surrounding air into the boundary layer or the surface of the droplet. This constantly removes the evaporated vapor from the interface and brings fresh ambient air into the interface. Also as reported by the previous studies [20,29] there is a possibility of formation of the internal boundary layer on the surface of droplet due to the internal circulation. Effectively the modified surface temperature due to these phenomena will alter the evaporation kinetics. The replacement of the evaporated vapor and the modification of the surface temperature are considered to be the main mechanism responsible for enhancement in evaporation.

D. Theoretical scaling analysis of various convection mechanisms

1. Thermal Marangoni and Rayleigh convection in liquid

Internal fluid motion or circulation may be produced within a freely suspended hanging evaporating droplet due to the presence of unbalanced forces or transport gradients either on the droplet surface or within the bulk. For internal circulation to manifest, a thermal gradient is expected to be present within the droplet. The gradient then drives heat conduction and the convective current

due to the internal circulation, the net effect of which is balanced by the enthalpy flux due to mass transport from the surface of the evaporating droplet to the ambient. The energy may be expressed as [20]

$$\dot{m} h_{fg} = k_{\text{th}} A \frac{\Delta T_m}{R} + \rho C_p u_{c,m} \Delta T_m A, \tag{2}$$

where, K_{th} is the thermal conductivity of the fluid droplet, A is the area, R is the droplet radius, and ΔT_m is the temperature difference. The sum of these two contributing factors will yield the total evaporation energy. The scale of internal circulation velocity magnitude due to the thermal Marangoni convection may be expressed as $u_{c,m} = (\frac{\sigma_T \Delta T_m}{\mu})$. Using the above scaled velocity and expressing the mass evaporation rate in terms of the droplet size reduction rate, Eq. (2) can be expressed as

$$R\rho \dot{R} h_{fg} = \Delta T_m k_{\text{th}} [1 + \text{Ma}], \tag{3}$$

where $\dot{R}$ is the rate of change of the spherical equivalent radius of the droplet, and Ma denotes the Marangoni number responsible for surface tension gradient-generated circulation by virtue of temperature gradient across the droplet and is expressed as $\text{Ma} = \frac{\sigma_T \Delta T_m R}{\alpha^* \mu}$ where σ_T denotes the derivative of surface tension as a function of temperature, i.e., $\sigma_T = \frac{d\sigma}{dT}$, α^* denotes the thermal diffusivity and μ denotes the viscosity of the droplet fluid. The equation is rearranged to obtain the driving potential for the circulation assuming $1 + \text{Ma} \sim \text{Ma}$ [20,32] (assuming that the similar criteria hold good for complex fluids also) in terms of the experimentally observed parameters and the thermophysical properties as (see the Supplemental Material for detailed derivation [23])

$$\Delta T_m = \sqrt{\frac{\dot{R} h_{fg} \mu}{\sigma_T C_p}}. \tag{4}$$

Hence the thermal Marangoni number can be expressed as

$$\text{Ma}_T = \frac{R}{\alpha} \sqrt{\frac{\dot{R} h_{fg} \sigma_T}{C_p \mu}}. \tag{5}$$

Similarly, the temperature difference existing between the droplet surface and the bulk also leads to buoyancy-driven convective currents within the droplet, leading to changed evaporation kinetics. A similar analysis of energy balance with a velocity scale of $u_{c,r} = (\frac{g\beta \Delta T_r R^2}{\nu})$ (where $u_{c,r}$ represents the internal circulation velocity by virtue of buoyancy-driven forces) gives the expression for Rayleigh number in terms of known parameters as

$$\text{Ra} = \frac{R^2}{\alpha} \sqrt{\frac{g\beta\rho \dot{R} h_{fg}}{\mu C_p}}. \tag{6}$$

Hence the Marangoni and Rayleigh numbers can be elucidated based on the experimental and thermophysical properties of the evaporating fluid for all the cases of the aqueous surfactant solutions, nanocolloids, and surfactant-infused nanocolloids.

2. Solutal Marangoni convection in a droplet

For the solutal effect to come into picture, a concentration gradient is an essential requirement. Performing a similar scaling analysis for the rate of evaporation of the droplet, we can write that the total rate of evaporation is caused due to the diffusive flux of mass transfer across the radius of the droplet with a concentration gradient of ΔC_m and due to a convective current of mass diffusion. Hence the total species transport balance can be expressed as

$$\dot{m} = DA \frac{\Delta C_m}{R} + u_{c,m} \Delta C_m A, \tag{7}$$

where D is the diffusion coefficient, R is the droplet radius and $u_{c,m}$ is the magnitude of the internal circulation current. The magnitude of the internal solutal convective current can be expressed as

$$u_{c,m} = \left(\frac{\sigma_C \Delta C_m}{\mu}\right), \tag{8}$$

where σ_c is the rate of change of surface tension with concentration and μ is the dynamic viscosity. Hence Eq. (7) can be expressed as (see the Supplemental Material for details [23])

$$\rho R \dot{R} = \Delta C_m D[1 + \mathrm{Ma}_s], \tag{9}$$

where the solutal Marangoni number is defined as [33] $\mathrm{Ma}_s = \frac{\sigma_C \Delta C_m R}{D\mu}$ and assuming $(1 + \mathrm{Ma}_s) \sim \mathrm{Ma}_s$ [34] the equation can be rearranged to obtain the concentration difference as

$$\Delta C_m = \sqrt{\frac{\rho \dot{R} \mu}{\sigma_C}}. \tag{10}$$

Hence the solutal Marangoni number can be expressed using the definition for the concentration difference from the above equation as

$$\mathrm{Ma}_s = \frac{R}{D}\sqrt{\frac{\rho \dot{R} \sigma_C}{\mu}}. \tag{11}$$

Hence the concentration gradient Marangoni can now be estimated for different complex fluids considered. The estimate of the different possible convection mechanisms will give rise to proper understanding of the physics of the problem.

The present experiments are conceived in such a manner so that the effect of stray convection is minimal. Even in the absence of any stray external convection, the thermal buoyancy can possibly trigger natural convection. But as the present analysis of different fluids evaporating is compared with respect to the water evaporating at the same conditions the effect of external convection can be neglected. However, in order to get a rough estimate of the effect of thermal buoyancy-driven convection, a rough estimate of Rayleigh number is presented. The expression for the Rayleigh number corresponding to thermal convections in the gas phase can be expressed as

$$\mathrm{Ra} = \left(\frac{g \beta_a \Delta T_{\mathrm{avg}} R^3}{\nu_a \alpha_a}\right), \tag{12}$$

where ΔT_{avg} is the temperature difference between the drop surface and the surrounding gas and ν_a and α_a are the kinematic viscosity and the thermal diffusivity of the surrounding gas, respectively. A rough estimate of the Rayleigh number was obtained to be very low around ~10–15, indicating that the buoyancy-driven convection if any will be very weak under the present experimental conditions. Hence the influence of convection due to the surrounding gas on the droplet evaporation kinetics is assumed to be negligible.

E. Stability analysis and mechanism of internal circulation

Figure 8 illustrates the thermal Marangoni versus Rayleigh number stability map for different complex fluids considered. The thermal Marangoni and Rayleigh number are estimated for the aqueous surfactant solutions at different concentrations of the surfactant are represented in Fig. 8(a). It can be observed that as the surfactant concentration increases, the Marangoni and the Rayleigh numbers increase up to the micellar concentration, and thereafter in the postmicellar concentration there is only marginal change.

The stability curve 1 represents the stability criteria as per Nield [32] from the linear theory, and the stability curve 2 represents the boundary condition proposed by Davis [34] from the energy theory. The stability of the buoyancy-surface tension-driven flows can be evaluated from the Marangoni number versus the Rayleigh number plot. The energy theory gives a more rigorous boundary for stability

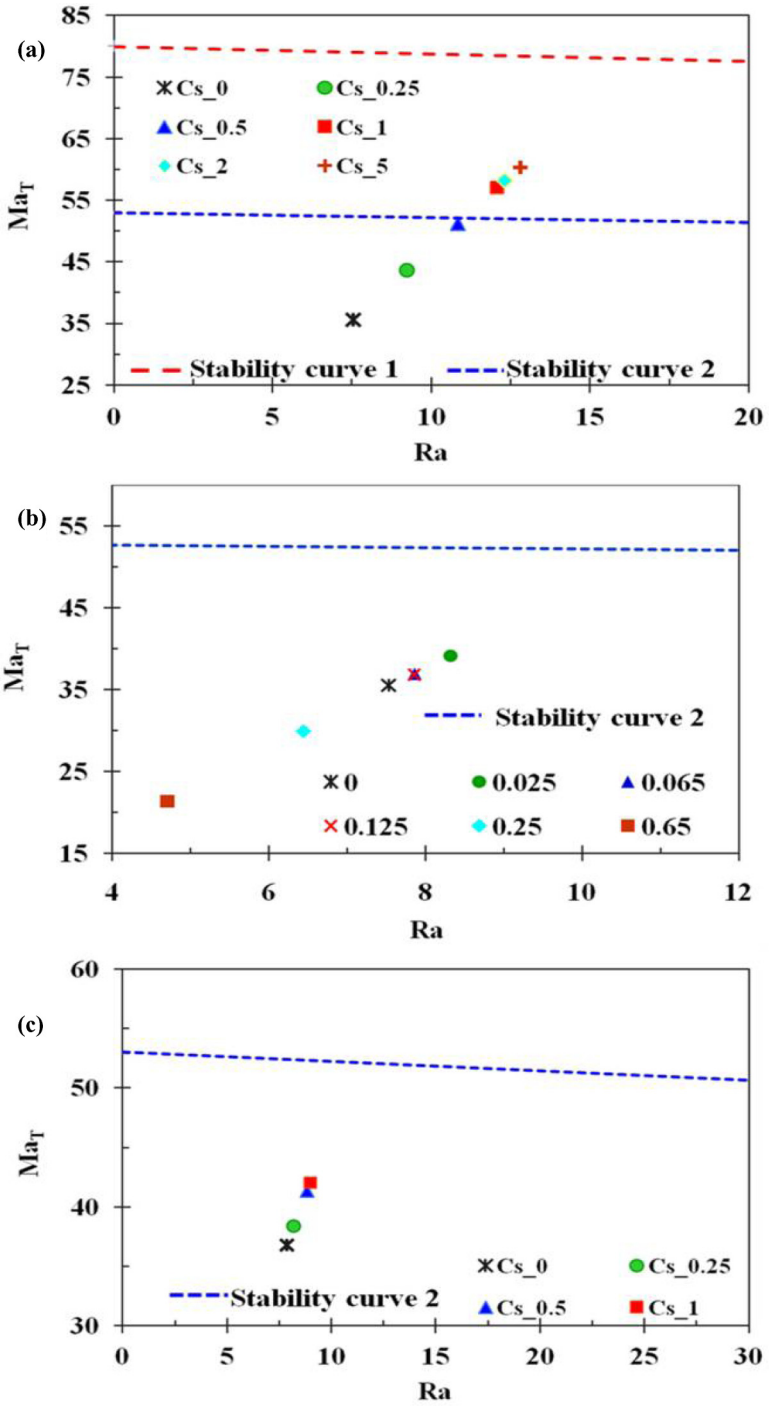

FIG. 8. Thermal Marangoni number versus Rayleigh number stability plot with the stability boundary lines (stability curve 1 indicates that boundary proposed by Nield [32] and stability curve 2 indicates that proposed by Davis [34]) with water and (a) aqueous surfactant solutions at different concentrations, (b) nanocolloids of only particles at different particle concentration, and (c) surfactant-impregnated nanocolloids at a particle concentration of 0.025 vol% and at different surfactant concentrations.

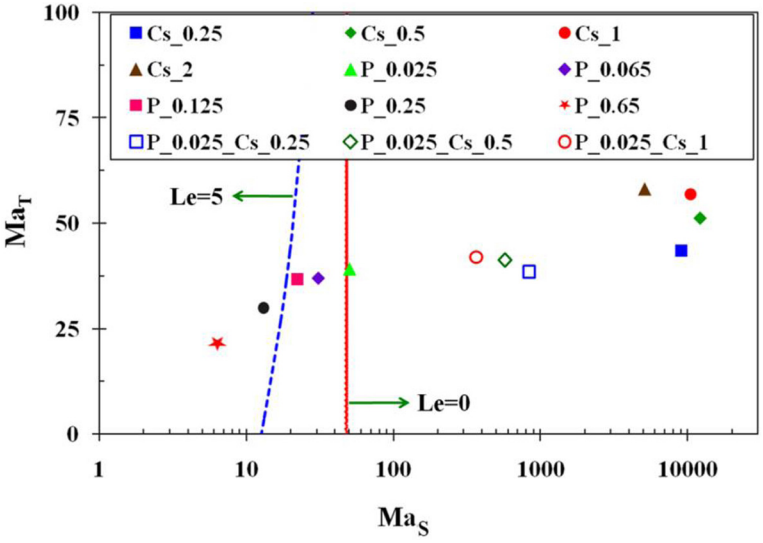

FIG. 9. Thermal Marangoni number versus the solutal Marangoni number plot with the stability curves at different Lewis numbers proposed by Joo [35] indicating the loci of points for different complex fluids considered.

and gives the sufficient condition for stability. It can be observed that the surfactant solutions below surfactant concentration of $C_s = 0.5$ fall below the stability line and represent a weak circulation, whereas the surfactant concentration of $C_s = 0.5$ and more just crosses the boundary proposed by energy theory. The points in between these two stability curves represent the zone of subcritical instabilities and exhibit a considerable circulation. This validates the experimental flow visualization observations as described earlier. However, we are observing a considerable circulation in the case of aqueous surfactant solutions even at a concentration of $C_s = 0.25$, which calls for another mechanism which drives the convection current. Figure 8(b) indicates the same stability criteria applied to the only nanoparticle colloidal solutions. As the particle concentration increases initially the Marangoni and Rayleigh numbers increase and then decrease after particular concentration. But it is interesting to note that none of the points crosses the stability boundary line, and this can be ascribed to be the reason for observing a weak circulation in the case of nanocolloidal solutions. It can be observed that as the particle loading increases, the convection currents decrease. Figure 8(c) illustrates the stability curve plot for surfactant-impregnated nanocolloids. It can be observed that the Marangoni and Rayleigh numbers have slightly increased from that of the water case, but the points do not cross the energy stability criteria. However, we are observing a strong convection current in the case of combined surfactant and nanocolloidal systems. Hence it can be elucidated that there is another convection mechanism which plays a role in enhancing the evaporation kinetics.

The stability criteria for the solutothermal convection where both the solutal and the thermal Marangoni convection are present can be evaluated from the thermal Marangoni number versus the solutal Marangoni number stability plot as proposed by Joo [35]. Figure 9 illustrates the thermal Marangoni number versus the solutal Marangoni number plot with the stability curves at different Lewis numbers for aqueous surfactant solution at different surfactant concentrations, nanocolloidal solutions at different particle concentrations, and combined surfactant and particle colloids at different surfactant concentrations at a given particle concenration of 0.025 vol%. The Lewis number for the present experimental case can be expressed as $\mathrm{Le} = \frac{k_{\mathrm{th}}}{\rho_g D C_{pg}}$, where K_{th}, ρ_g, and C_{pg} are the thermal conductivity, density, and specific heat of the surrounding gas, respectively. The solutal and thermal Marangoni number are evaluated based on the theoretical analysis presented above.

An estimate of the Lewis number for the present experimental case came out to be 0.8. As per the stability criteria proposed by Joo [35], the stability curves for Le = 0.8 and Le = 0 coincide with each other for the range of Marangoni numbers considered in the present study. It can be observed that surfactant solutions of all concentrations are far away from the boundary line and fall in the unstable regime of the map and thus have the potential for exhibiting a strong solutothermal convection. The solutal Marangoni number increases and then decreases after the micellar concentration in the case of surfactant solutions. The surfactant-infused nanocolloids also lie in the unstable regime of the stability map, thus exhibiting a strong solute-thermal convection. The enhanced evaporation of the aqueous surfactants and surfactant-impregnated nanocolloids can be attributed to the augmented solute-thermal convection. However, it is observed that with the increase in surfactant concentration for a given particle concentration, the solutal Marangoni number decreases. It may be due to the fact that as the surfactant concentration increases, the steric hindrance at the interface enhances, which may hamper the convection current generated due to the diffusion of combined surfactant and particles [7]. The nanocolloids of only particle systems also lie in the zone of unstable region in the stability map, thus implying possible potential solutothermal convective currents in such systems theoretically. Also this is supported by a weak circulation observed experimentally in nanocolloidal solutions at a very low particle concentration. The present approach is based on the assumption that the stability criteria for the normal fluids are valid in the case of complex fluids also as there is no literature available on the stability criteria for complex fluids. As the particle loading increases, the solutal and thermal Marangoni number decreases and the points move towards a stable region, which may be due to the enhanced viscous dissipation.

Hence from the theoretical stability map analysis, it can be established that solutothermal convective current is the main mechanism which is responsible for the observed enhancement of evaporation rate in aqueous surfactants, nanocolloids, and surfactant-infused nanocolloids. However, the mechanism and the degree of contribution of this are slightly different for different fluids as explained below. In aqueous surfactant solutions, due to the Gibbs adsorption of surfactants at the interface will result in surface pressure due to surface excess [7], and this increases as the evaporation proceeds, which will trigger back diffusion. Also the orientational difference and unequal distribution of surface excess of surfactant at the interface creates a surface tensional gradient which is potent enough to stimulate a convection current inside the droplet. With an increase in surfactant concentration, the gradient increases and enhances the convective current (see the Supplemental Material for graphical illustration [23]). This reversal in direction in some cases can also be considered as the end result of the complex surfactant molecule rearrangement and the adsorption-desorption characteristics locally modulating the surface tensional gradient. After micellar concentration, the aggregated micelles are no longer capable of locally altering the surface tension gradients, and hence any change in the convection pattern which is in accordance with the experimentally observed evaporation rate proves our hypothesis. The main mechanism triggering the circulation and hence enhancement in surfactant-infused nanocolloids is the solutothermal convection. As from the previous study [7], due to the surfactant-nanoparticle interaction, the surfactant-capped nanoparticles are driven to the interface hence by enhancing the surfactant population at the interface which results in a strong convection current compared to the aqueous surfactant case. The oscillatory convection current is generated due to the convective driving potential imparted due to the surfactant effect and retarding or retracting effect due to the particle effect as the particle loading enhances the viscous effect and tries to retard the motion. This results in the localized concentration gradient and sets the droplet in oscillatory convective motion. We have seen the complexing and noncomplexing nanocolloidal evaporation rate. In a complexing system, the surfactant-capped nanoparticle are driven to interface and hence by populating the interface and reducing the surface tension even further, and this facilitates the water molecules to leave the surface as it reduces the surface energy. Also, this promotes high solutal Marangoni as described. This enhances the evaporation. In a noncomplexing system, the surfactant effect is dominating as an electrostatic interaction between particle and surfactant is absent in this system and hence lacks nanoparticle-driven adsorption to interface. Hence this exhibits evaporation rate lower than complexing systems. In nanocolloidal solutions of particle, as

theoretically predicted, the solutothermal convection currents is the main factor behind enhancement. But this is limited by the experimental proof at higher concentrations due to the limitation in performing flow visualization. A weak solutothermal Marangoni (as observed experimentally) arising out of the localized concentration difference at an extremely low concentration proves this. The shear stress promoted by the circulation current at the fluid surface due to the particle movement will constantly entrain and replenish the surrounding gas at the interface of the droplet. This will constantly remove the evaporated vapor from the interface and allow the fresh air to acquire vapor. Also the presence of particles can modify the droplet surface temperature. This will have a direct consequence on enhancement of the evaporation rate. Another factor which also can play a possible role in enhancement is the increment in the effective diffusivity ratio due to addition of nanoparticles. Nanofluids are reported to exhibit higher diffusivity by at least one order of magnitude when compared to the base fluids [36]. This effectively leads to enhanced mass transfer or species transport characteristics in nanofluids. This enhanced diffusivity has a direct influence on the agitated movement of nanoparticles in the droplet, and this is directly linked to the effective diffusion of the particles' random Brownian motion and an enhanced thermophoretic drift due to enhancement in thermal conductivity inside the droplet. So this process enhances the strength of the random movement within the droplet, thereby influencing the evaporation rate in the case of nanofluids. The effective diffusion coefficient ratio has been reported to increase with increase in the particle concentration [36]. It is observed that the evaporation rate ratio also exhibits a similar trend of increase with the increase in particle concentration and the trend of increment is quite similar to the diffusivity ratio. In the present study, along with the evaporation rate of the pendant drops as a function of time, the simultaneous measurement of the surface tensions of the drops are also deduced so to understand the surface compression due to adsorption and hence thereby understanding the solutal Marangoni convection observed in different cases. However, initial transient response gives an insight into the physics of adsorption, but the late regimes result in erroneous surface tension due to the change in pendant shape due to considerable volume loss. See the Supplemental Material for details [23,37,38].

The velocity estimates for the present study from the solutothermal convection from the theoretical scaling analysis match quite well with that observed experiemntally (from the flow visualization technique) for the aqueous surfactant solutions as illustrated in Fig. 10(a) for various concentrations of the surfactants in both the premicellar and post-micellar regions.

Towards a higher concentration of surfactants, the match is quite appreciable. The match between the theoretical and the experimentally observed velocity indicates that the solutothermal Marangoni is the main driving potential behind the enhanced evaportation kinetics of aqueous surfactant solutions. No appreciable change in the velocity of circulation is observed in the postmicellar region possibly due to the saturation in the value of σ_c. The nature of the root-mean-square variation of the theoretical solutothermal convection velocity and experimentally observed velocity in the case of the surfactant-infused nanocolloidal solution is illustrated in Fig. 10(b). The theoretical calcuations match the experimental observations quite well and hence validate the theoretical analysis.

IV. CONCLUSION

In summary the present work shows that there exists an internal circulation in aqueous surfactant pendant droplets, nanocolloidal droplets, and combined surfactant-impregnated nanocolloidal pendant droplets. The rate of evaporation enhances with surfactant concentration and particle concentration for all the fluids studied. The evaporation rate is a stong function of the surfactant concentration up to the micellar concentration, and it is insensitive after the micellar concentration. The rate of evaporation enhanced with the use of nanocolloidal solutions of only particles and the rate is a strong function of the concentration of the particles. The combined surfactant and nanoparticle nanocolloidal sytems showed the maximum enhancement in evaporation rate and the rate of evaporation increases with the particle concentration at a given surfactant concentrtioin and also with the surfactant concentration at a given particle concentration. An oscillatory convection

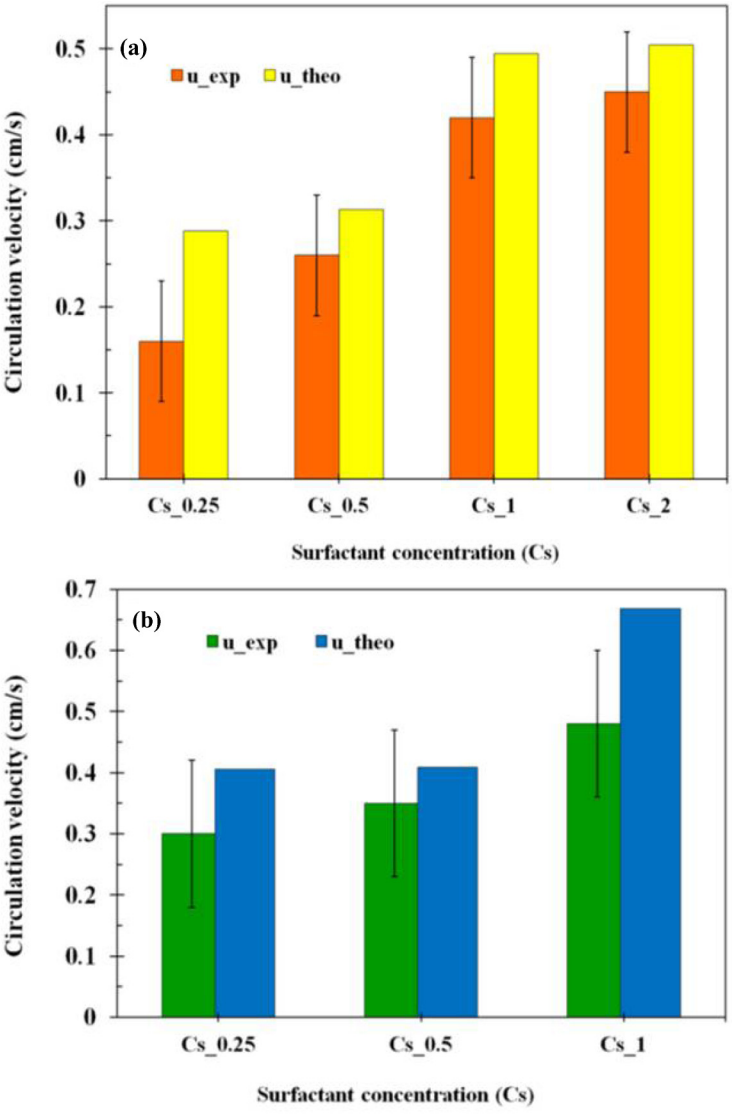

FIG. 10. Theoretical mean velocity from the calculations (u_{theo}) and the experimentally observed velocity (u_{exp}) for (a) aqueous SDS solutions at different concentration of the surfactants and (b) CTAB-infused Al_2O_3 nanocolloids at various concentration of the surfactant at a given particle concentration of 0.025 vol%.

pattern was found to be responsible for the enhancement in the evaporation characterestics in surfactant-impregnated nanocolloidal systems. A weak Marangoni convection together with enhnaced diffusivity and the enhanced Brownian and thermophoresis was found to be responsible for enhancement in the evpoartion kinetics of particle-laden micropendant droplets. The solutothermal Marangoni was found to be responsible for enhancement in the evaporation rate in an aqueous surfactant and combined surfactant nanocolloidal droplets. The theoretical analysis revealed the Marangoni-Rayleigh convection in the fluid from stability map. The present study brings out the physics behind the enhancement in interfacial mass transport in surfactant-impregnated complex fluids.

ACKNOWLEDGMENTS

A.R.H. would also like to thank Ministry of Human Resources, Government of India for a doctoral scholarship. P.D. thanks IIT Ropar for financial support towards the present study (Grants No. IITRPR/Research/193 and No. IITRPR/Interdisp/CDT). The authors declare no conflict of interest with any individual or agency.

A.R.H. planned and conducted the experiment and prepared the manuscript. A.R.H., P.D., S.G., and S.K.D. discussed and assisted in data analysis. P.D., S.G., and S.K.D. proofread the manuscript.

[1] R. Savino and S. Fico, Transient Marangoni convection in hanging evaporating drops, Phys. Fluids **16**, 3738 (2004).

[2] C. K. Law, Recent advances in droplet vaporization and combustion, Prog. Energy Combust. Sci. **8**, 171 (1982).

[3] S. Somasundaram, T. N. C. Anand, and S. Bakshi, Evaporation-induced flow around a pendant droplet and its influence on evaporation, Phys. Fluids **27**, 112105 (2015).

[4] H. Y. Erbil, Evaporation of pure liquid sessile and spherical suspended drops: A review, Adv. Colloid Interface Sci. **170**, 67 (2012).

[5] R. D. Deegan, Pattern formation in drying drops, Phys. Rev. E **61**, 475 (2000).

[6] K. Sefiane, S. K. Wilson, S. David, G. J. Dunn, and B. R. Duffy, On the effect of the atmosphere on the evaporation of sessile droplets of water, Phys. Fluids **21**, 062101 (2009).

[7] A. R. Harikrishnan, P. Dhar, P. K. Agnihotri, S. Gedupudi, and S. K. Das, Effects of interplay of nanoparticles, surfactants and base fluid on the surface tension of nanocolloids, Eur. Phys. J. E **40**, 53 (2017).

[8] A. R. Harikrishnan, P. Dhar, P. K. Agnihotri, S. Gedupudi, and S. K. Das, Wettability of complex fluids and surfactant capped nanoparticle-induced quasi-universal wetting behaviour, J. Phys. Chem. B **121**, 6081 (2017).

[9] D. H. Kumar, H. E. Patel, V. R. Kumar, T. Sundararajan, T. Pradeep, and S. K. Das, Model for Heat Conduction in Nanofluids, Phys. Rev. Lett. **93**, 144301 (2004).

[10] A. R. Harikrishnan, S. K. Das, P. K. Agnihotri, and P. Dhar, Particle and surfactant interactions effected polar and dispersive components of interfacial energy in nanocolloids, J. Appl. Phys. **122**, 054301 (2017).

[11] R. G. Picknett and R. Bexon, The evaporation of sessile or pendant drops in still air, J. Colloid Interface Sci. **61**, 336 (1977).

[12] R. D. Deegan, O. Bakajin, T. F. Dupont, G. Huber, S. R. Nagel, and T. A. Witten, Capillary flow as the cause of ring stains from dried liquid drops, Nature (London) **389**, 827 (1997).

[13] Y. O. Popov, Evaporative deposition patterns: Spatial dimensions of the deposit, Phys. Rev. E **71**, 036313 (2005).

[14] C. H. Chon, S. Paik, J. B. Tipton, and K. D. Kihm, Effect of nanoparticle sizes and number densities on the evaporation and dryout characteristics for strongly pinned nanofluid droplets, Langmuir **23**, 2953 (2007).

[15] R. H. Chen, T. X. Phuoc, and D. Martello, Effects of nanoparticles on nanofluid droplet evaporation, Int. J. Heat Mass Transfer **53**, 3677 (2010).

[16] T. A. Nguyen and A. V. Nguyen, Increased evaporation kinetics of sessile droplets by using nanoparticles, Langmuir **28**, 16725 (2012).

[17] V. Garbin, J. C. Crocker, and K. J. Stebe, Nanoparticles at fluid interfaces: Exploiting capping ligands to control adsorption, stability and dynamics, J. Colloid Interface Sci. **387**, 1 (2012).

[18] H. S. Wi, S. Cingarapu, K. J. Klabunde, and B. M. Law, Nanoparticle adsorption at liquid–vapor surfaces: Influence of nanoparticle thermodynamics, wettability, and line tension, Langmuir **27**, 9979 (2011).

[19] W. J. Gerken, A. V. Thomas, N. Koratkar, and M. A. Oehlschlaeger, Nanofluid pendant droplet evaporation: Experiments and modelling, Int. J. Heat Mass Transfer **74**, 263 (2014).

[20] D. K. Mandal and S. Bakshi, Internal circulation in a single droplet evaporating in a closed chamber, Int. J. Multiph. Flow **42**, 42 (2012).
[21] S. Semenov, A. Trybala, H. Agogo, N. Kovalchuk, F. Ortega, R. G. Rubio, V. M. Starov, and M. G. Velarde, Evaporation of droplets of surfactant solutions, Langmuir **29**, 10028 (2013).
[22] X. Fang, A. B. Páhi, H. Li, and P. Somasundaran, Enhancement of water transport through the liquid–vapor interface by surfactants, Soft Matter, **8**, 8959 (2012).
[23] See Supplemental Material at http://link.aps.org/supplemental/10.1103/PhysRevFluids.3.073604 for the experimental details including SEM characterization of nanoparticles. Theoretical description of diffusion driven evaporation are also presented. Detailed scaling analysis of various convection mechanisms, mechanism of evaporation in various systems, details of theoretical analysis, and transient surface tension data are also presented.
[24] P. Dhar, M. H. D. Ansari, S. S. Gupta, V. M. Siva, T. Pradeep, A. Pattamatta, and S. K. Das, Percolation network dynamicity and sheet dynamics governed viscous behavior of polydispersed graphene nanosheet suspensions, J. Nanopart Res. **15**, 2095 (2013).
[25] N. Kurra, V. S. Bhadram, C. Narayana, and G. U. Kulkarni, Few layer graphene to graphitic films: Infrared photoconductive versus bolometric response, Nanoscale **5**, 381 (2013).
[26] W. Thielicke and E. Stamhuis, PIVlab—Towards user-friendly, affordable and accurate digital particle image velocimetry in MATLAB, J. Open Res. Softw. **2**, e30 (2014).
[27] C. A. Schneider, W. S. Rasband, and K. W. Eliceiri, NIH Image to ImageJ: 25 years of image analysis, Nat. Methods **9**, 671 (2012).
[28] M. M. Yovanovich, New Nusselt and Sherwood numbers for arbitrary isopotential bodies at near zero Péclet and Rayleigh numbers, in *Proceedings of the AIAA, 22nd Thermophysics Conference* (AIAA, Reston, VA, 1987), p. 1643.
[29] B. Abramzon and W. A. Sirignano, Droplet vaporization model for spray combustion calculations, Int. J. Heat Mass Transfer **32**, 1605 (1989).
[30] H. Ma, M. Luo, and L. L. Dai, Influences of surfactant and nanoparticle assembly on effective interfacial tensions, Phys. Chem. Chem. Phys. **10**, 2207 (2008).
[31] V. Garbin, I. Jenkins, T. Sinno, J. C. Crocker, and K. J. Stebe, Interactions and Stress Relaxation in Monolayers of Soft Nanoparticles at Fluid-Fluid Interfaces, Phys. Rev. Lett. **114**, 108301 (2015).
[32] D. A. Nield, Surface tension and buoyancy effects in cellular convection, J. Fluid Mech. **19**, 341 (1964).
[33] K. H. Kang, C. K. Choi, and I .G. Hwang, Onset of solutal Marangoni convection in a suddenly desorbing liquid layer, AIChE J. **46**, 15 (2000).
[34] S. H. Davis, Buoyancy-surface tension instability by the method of energy, J. Fluid Mech. **39**, 347 (1969).
[35] S. W. Joo, Marangoni instabilities in liquid mixtures with Soret effects, J. Fluid Mech. **293**, 127 (1995).
[36] S. Krishnamurthy, P. Bhattacharya, P. E. Phelan, and R. S. Prasher, Enhanced mass transport in nanofluids, Nano Lett. **6**, 419 (2006).
[37] J. D. Berry, M. J. Neeson, R. R. Dagastine, D. Y. C Chan, and R. F. Tabor. Measurement of surface and interfacial tension using pendant drop tensiometry. J. Colloid Interface Sci. **454**, 226 (2015).
[38] M. Hoorfar and A. W. Neumann, Recent progress in axisymmetric drop shape analysis (ADSA), Adv. Colloid Interface Sci. **121**, 25 (2006).